**UNIVERSIDADE FEDERAL DO PARÁ**
**INSTITUTO DE GEOCIÊNCIAS**
**PROGRAMA DE PÓS-GRADUAÇÃO EM GEOFÍSICA**

THAÍS ANGÉLICA DA COSTA BORBA

**MODELAGEM HIDRODINÂMICA APLICADA AO ESTUÁRIO AMAZÔNICO:** UMA
ABORDAGEM EM MALHA FLEXIVEL.
**(HYDRODYNAMIC MODELLING IN AMAZONIAN ESTUARY**: A FLEXIBLE MESH
APPROACH)

**BELÉM**
**2014**

THAÍS ANGÉLICA DA COSTA BORBA

**MODELAGEM HIDRODINÂMICA APLICADA AO ESTUÁRIO AMAZÔNICO:**
UMA ABORDAGEM EM MALHA FLEXIVEL.
**(HYDRODYNAMIC MODELLING IN AMAZONIAN ESTUARY**: A FLEXIBLE
MESH APPROACH)

Dissertação apresentada ao Programa de Pós-Graduação em Geofísica do Instituto de Geociências da Universidade Federal do Pará em cumprimento às exigências para a obtenção de título de Mestre em Geofísica.
Área de Concentração: Geofísica Marinha
Orientador: Prof. Dr. Marcelo Rollnic

**BELÉM**
**2014**

THAÍS ANGÉLICA DA COSTA BORBA

**MODELAGEM HIDRODINÂMICA APLICADA AO ESTUÁRIO AMAZÔNICO:** UMA
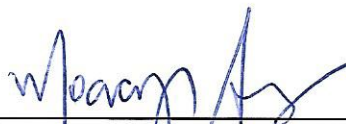ABORDAGEM EM MALHA FLEXIVEL.

> Dissertação apresentada ao Programa de
> Pós-Graduação em Geofísica do  Instituto
> de Geociências da Universidade Federal do
> Pará em cumprimento às exigências para a
> obtenção de título de Mestre em Geofísica.

Data de Aprovação: 19 / 08 / 2014

Banca Examinadora:

_____
Prof. Dr. Marcelo Rollnic - Orientador
Doutor em Oceanografia
Universidade Federal do Pará

_____
Prof. Dr. Moacyr Cunha de Araujo Filho
Doutor em Física e Química do Meio Ambiente
Universidade Federal de Pernambuco

_____
Prof. Dr. Nils Edvin Asp Neto
Doutor em Geologia Costeira
Universidade Federal do Pará

# RESUMO

O estuário amazônico é um complexo sistema devido ao grande número de corpos d'água que apresenta; este estuário também compreende quatro dos 20 maiores rios do mundo. Modelos hidrodinâmicos já foram aplicados a este sistema, mas sua complexa morfologia torna difícil a definição de grides curvilineares para a área. O presente trabalho de pesquisa tem como objetivo a implementação de modelo hidrodinâmico no estuário amazônico, baseado em malha flexível (cuja definição é mais simples do que das curvilíneares para sistemas com tal complexidade), além de analisar alguns de seus padrões hidrodinâmicos. A metodologia é baseada na utilização do modelo D-Flow em que a definição de malha flexível é possível. O modelo abrange os baixos cursos do Rio Amazonas, do Rio Tapajós, do Rio Xingu, do Rio Tocantins, da Baía do Guajará, da Baía do Marajó, do Estreito de Breves e do Rio Pará, bem como a planície de maré circundante e a plataforma continental adjacente. O modelo apresentou bons valores de calibração, tanto para maré quanto para descarga fluvial, uma vez que o coeficiente de correlação de Pearson apresentou valores superiores a 0,95 e o erro médio foi menor do que 5% pra resultados de maré e 15% para os resultados de descarga. O modelo gerou uma representação da interação da maré e descarga fluvial relativa a condições extremas no estuário, mostrando padrões hidrodinâmicos aceitáveis quando comparados com medições realizadas "*in situ*".


**Palavras-chave:** D-Flow FM, coeficiente de Manning, descarga líquida, maré, malha flexível.

**ABSTRACT**

Amazonian Estuary is a very complex system due to its large number of water bodies; it also encompasses four of the 20 largest rivers of world. Several hydrodynamic models have been applied on this system, but its complexity on shape makes difficult the grid definition when curvilinear grid is used. This research aimed the implementation of hydrodynamic model on this, based in flexible mesh grid that is easier to define on this kind of systems than curvilinear grids, and analyze the hydrodynamic patterns within this estuary. The methodology is based on the use of D-Flow in which a flexible mesh can be defined. The model domain encompasses the low course of Amazon River, Tapajós River, Xingu River, Tocantins River, Guajará Bay, Marajó Bay, Breves Strait and Pará River as well as the flood plain area and the adjacent continental shelf. The model presents a quite good calibration values for tidal signal as well as discharge since the Pearson's correlation coefficient presented values bigger than 0.95 for both and rmse presented values smaller than 5% for the former and 15% for the latter. The model also performed well on representation of several scenarios that represented extreme conditions regarding tide and discharge sources of Amazonian Estuary and it showed expected patterns by comparison with *in situ* data.

**Keywords:** D-flow FM, Manning's coefficient, net discharge, tide, flexible mesh.

# LISTA DE ILUSTRAÇÕES

# LISTA DE TABELAS

# SUMÁRIO

## CAPÍTULO 1 APRESENTAÇÃO

Este trabalho é apresentado em forma de artigo, de acordo com as regras do Programa de Pós-Graduação em Geofísica da Universidade Federal do Pará. A formatação se apresenta de acordo com aquela descrita para submissão de artigos da revista Journal of Geophysical Research: Oceans presente no website http://publications.agu.org/author-resource-center/author-guide/.

A dissertação é dividida em três capítulos: o primeiro se limita à uma breve apresentação sobre o que vai ser discutido durante a dissertação; o segundo traz uma nota de setup e calibração que não se aplica na apresentação do artigo mas é fundamental para o entendimento do processo de modelagem e para futuras implementações de modelo na região; e o terceiro apresenta o artigo a ser enviado à publicação.

Um estuário pode ser definido com uma área transição em que o rio deságua no oceano. Esse sistema é regido por vazões fluviais e por gradientes de pressão que são criados por movimento de maré e variações de densidade na água.

Estuários são importante fonte de sedimentos e nutrientes provenientes do continente para os oceanos. A circulação hidrodinâmica mantem uma grande parte deste material dentro do estuário, consequentemente, estuários, com algumas exceções, são mais produtivos do que os rios e oceano adjacente (MIRANDA; CASTRO; KJERFVE, 2002). Eles são ambientes únicos devido aos gradientes de salinidade que são formados pela a diluição da água do mar pela água doce. Esse conjunto de características permite que ecossistemas como manguezais e marismas se desenvolvam tornando os estuários ecossistemas biologicamente ricos, abrigando diversas espécies.

Além da importância biológica os estuários têm grande importância econômica e social. Devido à riqueza biológica e localização, diferentes atividades podem ser desenvolvidas em um estuário, como, por exemplo, pesca, turismo e aquicultura. Atividades portuárias também são muito comuns, visto que estuários são rotas naturais que levam as redes fluviais. Essas características fazem dos estuários ambientes propícios para o homem, por isso seus entornos são habitados por grande parte da população mundial.

O estuário amazônico é composto por vários corpos de água dentre eles os rios Amazonas, Tapajós, Xingu e Tocantins, listados entre os 20 maiores rios do mundo (DAI; TRENBERTH, 2002). Esse estuário deságua na plataforma continental com uma descarga de aproximadamente 7,28 x 1012 m3/ano (MIKHAILOV, 2010).

Atualmente, várias técnicas de modelagem hidrodinâmica têm sido aplicadas no Estuário Amazônico, dentre elas: Nikiema, Devenon & Baklouti (2007) e Vinzon & Paiva (2002) usam estas técnicas principalmente para investigar a hidrodinâmica na plataforma continental, incluindo descarga fluvial e transporte sedimentar; Gabioux, Vinzon & Paiva (2005) investigam, por sua vez, a propagação de maré aplicando a modelagem em larga escala. Entretanto, malhas curvilineares, amplamente utilizadas nesses modelos, não são fáceis de serem definidas devido ao grande número de corpos d'água e planícies de maré que estão presentes no Estuário Amazônico. Esta dissertação de mestrado tem como objetivo implementar um modelo hidrodinâmico nesse estuário utilizando uma malha flexível (posteriormente descrita) afim de determinar alguns de seus padrões hidrodinâmicos.

## CAPÍTULO 2 NOTAS DE SETUP E CALIBRAÇÃO

### 2.1. Modelo

D-Flow FM foi utilizado para simular a hidrodinâmica do Estuário Amazônico (aqui descrito como a área que abrange os baixos cursos dos rios Amazonas, Tocantins, Tapajós e Xingu, além da Baía do Marajó, Baía do Guajará, Rio Pará, Estreito de Breves, planície de maré circundante e plataforma continental adjacente). D-FLow FM é um pacote de simulação hidrodinâmica em 1D-2D-3D que até a defesa dessa dissertação ainda estava sendo desenvolvida.

Descrição mais detalhada sobre D-Flow FM pode ser encontrada em Kernkamp *et al.* (2011), entretanto, ressalta-se a maior vantagem de se utilizar este pacote de simulação: a possibilidade de se definir um malha flexível, ou seja, um grid que combina uma malha curvilínea (elementos quadrangulares) com elementos triangulares, pentágonos, etc., além de canais 1D.

### 2.2. Domínio e Grid

A importância de se utilizar uma malha flexível no Estuário Amazônico é a configuração complexa de feições que variam tanto em tamanho quanto em forma. No Estuário Amazônico encontramos canais (sejam rios, canais ou canais de maré) que apresentam largura de alguns metros - canais do Estreito de Breves - bem como outros com largura de alguns quilômetros - Rio Amazonas.

O domínio abrange: os principais rios que estão localizados no Estuário Amazônico (Rio Amazonas, Rio Tapajós, Rio Xingu e Rio Tocantins); o Estreito de Breves e o Rio Pará (que são canais que comunicam o ramo oeste desse estuário com o seu ramo leste e que se localizam ao sul da Ilha do Marajó); as baías do Marajó e do Guajará; a planície de maré que circunda esses canais; e a plataforma continental adjacente.

O D-Flow FM não possibilita a correção da reflexão de maré nas fronteiras abertas referente aos rios, então, o domínio foi estendido até onde a maré dinâmica não é observada. As fronteiras abertas referentes ao oceano formam localizadas um pouco afastadas da área foco a fim de minimizar erros no modelo. Assim, o modelo cobre

cerca de 700 km ao longo da costa e 145 km offshore. No continente ele avança 716 km rio acima através do Rio Amazonas e 430 km rio acima através do Rio Tocantins.

A malha curvilínea foi definida para os canais dos rios Amazonas, Tapajós, Xingu e Tocantins, para a Baía do Marajó, Rio Pará e plataforma continental. Elementos triangulares foram definidos para a planície de maré, ilhas, e para comunicar os canais definidos em malha curvilínea. Canais em 1D foram definidos para o Estreito de Breves uma vez que os mesmos possuem largura muito inferior aos rios nos quais foi definida malha curvilínea.

O parâmetro de ortogonalidade referente tanto à suavidade (variação no tamanho dos elementos) quanto à ortogonalidade (ângulo entre os elementos) apresentou valor inferior a 0,06. Este parâmetro deve apresentar valor menor que 0,1. A malha flexível facilita o processo de ortogonalizar a malha, entretanto, este processo deve ser realizado por porções do grid e não aplicado a malha como um todo podendo gerar erros devido ao tamanho da malha e à falta de controle do processo.

## 2.3. Condições iniciais de setup

### 2.3.1. Batimetria

Devido à extensão do domínio, a batimetria foi obtida através de quatro fontes distintas: cartas náuticas, atlas náuticos, dados coletados e batimetria obtida por sensoriamento remoto disponível na base Delft Dashboard. Esse último disponibiliza a batimetria e os dados de elevação provenientes do GEBCO 08 que fornece a batimetria a partir de dados gerados pela combinação de medições de profundidade realizadas por navios e dados gravimétricos derivados de sensores orbitais (satélite). Para os dados terrestres, o GEBCO 08 utiliza o modelo de elevação digital SRTM30.

A batimetria foi definida em porções, dependendo da disponibilidade dos dados, começando pelos dados coletados, seguidos pelas cartas náuticas, pelo atlas e por fim pela batimetria adquirida na base Delft Dashboard. Essa última foi aplicada principalmente a planície de maré para a qual a carência de dados era maior.

## 2.3.2. Rugosidade

O coeficiente de rugosidade utilizado foi o de Manning. Inicialmente se propôs um coeficiente único para todo o domínio igual a 0,023. Em seguida, durante o processo de calibração foram definidos diferentes valores de Manning de acordo com a porção do domínio.

## 2.3.3. Descarga

Valores de descarga foram definidos para os rios Amazonas, Tapajós, Xingu e Tocantins a partir da série temporal presente no website da Agência Nacional das Águas (ANA). As séries contidas nesse banco de dados não são continuas, dessa forma se considerou 30 anos de dados a partir dos quais se calculou valores de médias de descargas mensais. As estações consideradas foram aquelas referentes às cidades de Óbidos, Itaituba, Altamira e Tucuruí.

## 3.4. Maré

Os dados de maré para alimentar os limites abertos do modelo referente ao oceano foram obtidos nos dados disponíveis no website do OTIS (discutido no capitulo 3) que se baseia em valores de altimetria. Inicialmente se adquiriu valores para todas as componentes de maré disponíveis a partir dessa fonte.

## 2.3.5. Vento

O vento varia tanto em espaço quanto em tempo dentro do domínio definido, entretanto, a fim de ter um maior controle do modelo, admitiu-se vento constante em espaço e tempo.

## 2.3.6. Setup de tempo

O modelo mostrou que precisa de tempo de simulação igual a 1 (um) mês para apresentar  equilíbrio quando o nível d'água inicial atribuído ao sistema é igual a zero. Assim, a simulação de calibração possui um tempo de simulação igual a dois meses, ou seja, um mês para o equilíbrio e outro para a calibração. O mês escolhido para a calibração foi o mês de julho, porque os dados disponíveis para a calibração são de descarga referente a esse mês.

Com base nos dados de descarga da ANA, para o período chuvoso se simulou o mês de maio e para o período seco se simulou o mês de novembro.

## 2.4. Calibração

Durante a calibração três principais parâmetros foram corrigidos, pois apenas com o setup inicial o modelo apresentou altos valores de erro principalmente na penetração da maré no estuário e descarga no Rio Pará. Os parâmetros são na ordem em que foram corrigidos durante o processo de calibração: batimetria, maré e rugosidade.

Vale ressaltar que a calibração se deu da plataforma para a parte continental. Assim os primeiros passos da calibração foram corrigir os valores de maré nas estações presentes na costa, seguidas por aquelas presentes no estuário e por fim os valores de descarga.

### 2.4.1. Batimetria

Devido alguns elementos do grid serem de tamanho grosseiro (da ordem de quilômetros), um mesmo elemento cobre feições diferentes, como por exemplo, uma barra arenosa e um canal, o que acaba por obstruir o fluxo da água no modelo. Assim, uma correção manual da batimetria foi necessária.

Para a correção da batimetria dos principais canais se determinou os valores batimétricos médios para algumas seções transversais e definiu-se um declive suave (o mais próximo possível da condição real). O processo foi feito para pequenas porções do domínio a fim de se ter um máximo controle da batimetria, respeitando as principais feições que ocorrem dentro do estuário.

A correção batimétrica também foi aplicada a plataforma continental para que a onda de maré fosse melhor propagada, assim, corrigindo valores principalmente de fase. Para essa correção foram apenas consideradas isolinhas de profundidade com taxa de variação de 5 m de profundidade.

### 2.4.2. Maré

Como descrito anteriormente, inicialmente se adquiriu valores para todas as componentes de maré disponíveis através do OTIS. Entretanto dados de calibração

mostraram que apenas as componentes de maré M2, S2, N2, K1, O1 e M4 ocorrem na porção mais externa da plataforma referente às fronteiras abertas no oceano. Dessa maneira, apenas essas componentes foram consideradas.

2.4.3. Rugosidade

Uma vez que o modelo já se encontrava parcialmente calibrado, após modificações nos dados de entrada de batimetria e maré, valores de rugosidade foram definidos. Estes dados tiveram grande importância para a calibração, pois corrigiram em até 20 cm valores de variação de nível d'água (maré) nos pontos de calibração.

Os valores de rugosidade foram baseados no manual apresentado por Arcementjr & Schneider (1989) como será descrito no **CAPÍTULO 3**.

## CAPÍTULO 3: ARTIGO

**Title:**

 HYDRODYNAMIC MODELLING IN AMAZONIAN ESTUARY: A FLEXIBLE MESH APPROACH.

**Authors:**

Thais A C Borba, Universidade Federal do Pará, Belém, Pará, Brazil.

Marcelo Rollnic, Universidade Federal do Pará, Belém, Pará, Brazil.

Corresponding author: T. A. C. Borba, Universidade Federal do Pará, Belém, Pará, Brazil. (tacborba@gmail.com)

**Key points**

The hydrodynamic of Amazon Estuary is simulated in a flexible grid.

Tide and discharge can be simulated by using of flexible grid for the Amazonian Estuary.

Expected hydrodynamic patterns were found.

**Abstract**

Amazonian Estuary is a very complex system due to its large number of water bodies; it also encompasses four of the 20 largest rivers of world. Several hydrodynamic models have been applied on this system, but its complexity on shape makes difficult the grid definition when curvilinear grid is used. This research aimed the implementation of hydrodynamic model on this, based in flexible mesh grid that is easier to define on this kind of systems than curvilinear grids, and analyze the hydrodynamic patterns within this estuary. The methodology is based on the use of D-Flow in which a flexible mesh can be defined. The model domain encompasses the low course of Amazon River, Tapajós River, Xingu River, Tocantins River, Guajará Bay, Marajó Bay, Breves Strait and Pará River as well as the flood plain area and the adjacent continental shelf. The model presents a quite good calibration values for tidal signal as well as discharge since the Pearson's correlation coefficient presented values bigger than 0.95 for both and rmse presented values smaller than 5% for the former and 15% for the latter. The model also performed well on representation of several

scenarios that represented extreme conditions regarding tide and discharge sources of Amazonian Estuary and it showed expected patterns by comparison with in situ data.

**Index terms and keywords**

 D-flow FM, Manning's coefficient, net discharge, tide, flexible mesh.

# 1. Introduction

Estuaries have biological, economic and social importance. Their dynamics and morphology allow that they shelter several biological species as well as allow the development of economic activities, for example, ports, fishing, tourism, and aquaculture. The combination of these characteristics has made estuaries very attractive for human life, thus they are usually widely populated.

The Amazon Estuary is composed by several water bodies in which the 4 biggest water bodies can be featured: Amazon River, Tapajós River, Xingu River and Tocantins River are in the group of the world's largest 20 rivers (DAI; TRENBERTH, 2002). This estuary flows into the continental shelf with a runoff about 7.28 x 1012 m3/year (MIKHAILOV, 2010).

A large number of water bodies are presented on Amazon Estuary as well as a large area of flood plain, for instance, Mertes, Dunne & Martinelli (1996) mentioned that the Amazon River floodplain is constituted of lakes, lakes deposits, floodplain channels, scroll bars, and overbank deposits.

Currently, several modelling techniques have been applied in Amazon River/Estuary system. Some examples are: Nikiema, Devenon & Baklouti (2007) and Vinzon & Paiva (2002), who use these techniques mainly to analyze the continental shelf dynamics including water runoff and sediment transport; Gabioux, Vinzon & Paiva (2005) made tidal propagation analyzes by apply modelling in large scale. Nevertheless, curvilinear mesh grid that is widely used on these models is not easily to be defined since a large number of water bodies are presented on Amazon Estuary as well as a large area of flood plain. This research aimed the implementation of hydrodynamic model on Amazon Estuary based in a flexible mesh grid that is easier to define on this kind of system than curvilinear grids, in order to analyze the hydrodynamic patterns within this estuary.

## 2. Methods

### 2.1 Physical area description

The Amazon River Basin is a tidal river. It is quite branched and has a funnel-shape, characteristics which are associated with estuaries (SIOLI, 1984). The funnel shape also makes possible to classify the Amazon River basin mouth as a coastal plain dominated by tide, in which the tidal currents are the main factor for morphological changes. Its estuarine area is driven by a semidiurnal mesotide and macrotide that penetrates into the estuary until distances of about 1000 km (Amazon River branch) from the coastal line (FEMAR, 2013).

It is composed of two main branches: the first, called Amazon River Estuary, flows in the west side of Marajó Island and flows into Atlantic Ocean most part of Amazon River water runoff; the second, called Pará River Estuary, is connected with the former by channels system called Breves Strait, which flows in the east side of Marajó Island and is fed by the Tocantins water system and Guajará Bay (Figure 1).
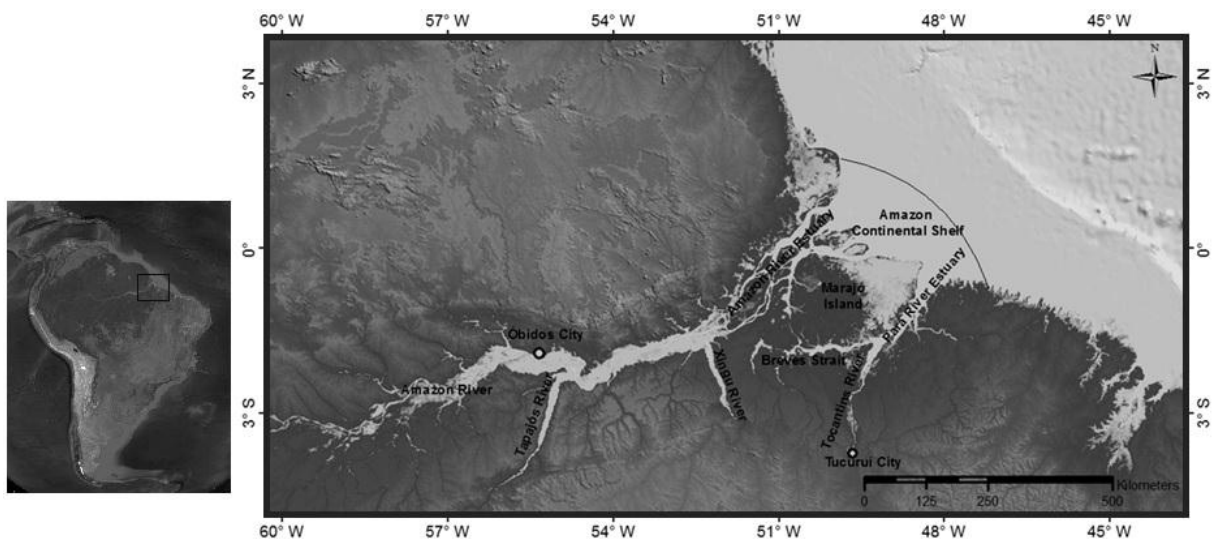


**Figure 1:** (left) Location of Amazon Estuary; (right) water bodies that constitute Amazon Estuary.

Regarding the circulation patterns, there are different classifications for this estuary. Some authors classify the estuary as a mixed estuary (BALTAZAR; MENEZES; ROLLNIC, 2011; BEZERRA et al., 2011). These authors usually consider measurements points inside the estuary until its mouth and salinity values less than 10. Nevertheless, some investigations on the adjacent continental shelf show that this estuary is a stratified system in which an estuarine plume was displaced to continental shelf due to high river system discharge (GEYER et al., 1996), where salinity values between 15 and 35 can be found.

The salinity gradients are mainly driven by the river discharge and tidal currents. The drainage of the Amazon River basin is very complex. It is formed by more than 500 larges rivers and uncountable others small water bodies (DAI; TRENBERTH, 2002), but this research was focused on the downstream area where the main tributaries are Tapajós River, Xingu River and Tocantins River. These rivers are described on Table 1.

**Table 1:** Main rivers characteristics (Source: Dai et al. (2002); Mikhailov (2010)).

| River | Total drainage area km$^2$ | Average annual discharge m$^3$ sec$^{-1}$ | Annual discharge km$^3$ year$^{-1}$ | Sediment Runoff t year$^{-1}$ |
|---|---|---|---|---|
| **Amazon (Obidos)** | $4.68 \times 10^6$ | $1.73 \times 10^5$ | 5460 | $1.26 \times 10^9$ |
| **Tapajos** | $5.02 \times 10^5$ | -* | 415 | -* |
| **Xingu** | $4.97 \times 10^5$ | $1.60 \times 10^4$ | 302 | $3.43 \times 10^6$ |
| **Tocantins** | $7.69 \times 10^5$ | $1.63 \times 10^4$ | 511 | $3.06 \times 10^6$ |

*no data

The rivers that flow into Amazon Estuary are fed mainly by rains. The climate in the study area is equatorial, hot and humid. The mean annual temperature, air humidity and annual rainfall are, respectively, 25 ºC, 80% and 2,889 mm/year. Considering all the Amazon Basin area, the maximum rate of atmospheric precipitation occurs between February and August, but the maximum rate of atmospheric precipitation into the estuarine area occurs in the period between February and May. Consequently the biggest river discharge occurs between the May and July, since it is expected that the river discharge changes due to the atmospheric precipitation rate with some delay (SIOLI, 1984; DAI; TRENBERTH, 2002; MIKHAILOV, 2010).

The estuary bathymetry is very irregular with presence of longitudinal sand bars and channels constructed by the tidal currents and river flow. The bathymetry values are around 20 m inside the estuary and reach 100 m on the continental shelf (but these values can reach values much bigger for both in some areas). Although the estuary is driven by tide, the waves play an important role by resuspension sediments and formation of estuarine beaches. Thus, the sediment distribution is a result of the combination of tidal currents, river currents and wave action in a small scale on the river banks (GREGÓRIO; MENDES, 2009).

The bottom sedimentology consists mainly of medium sand to clay. The coarse sediment grain size can be found in more internal part of the estuary; on the mouth portion in contact

with Atlantic Ocean, sediment can be found with finer grain size (COSTA; BOTTA; CARDILLE, 2003; CORRÊA, 2005; COSTA et al., 2013). Corrêa (2005) also describe a transversal variation of sediment grain size as results of ebb and flood currents during a tidal cycle.

## 2.2. Model

### 2.2.1. Domain and Grid

D-Flow Flexible Mesh was used to simulate the hydrodynamics of Amazon Estuary. It is a 1D-2D-3D hydrodynamic simulation package in development (until the conclusion of present research) by Deltares in cooperation with the Delft University of Technology, the Netherlands. It was based on numerical concepts of Delft3D and SOBEK1D2D, but the advantage of D-Flow Flexible Mesh is the possibility to define flexible mesh grids (Figure 2) that are curvilinear meshes combined with other grid elements, for instance, triangles and pentagons as well as 1D channel networks (KERNKAMP et al., 2011).
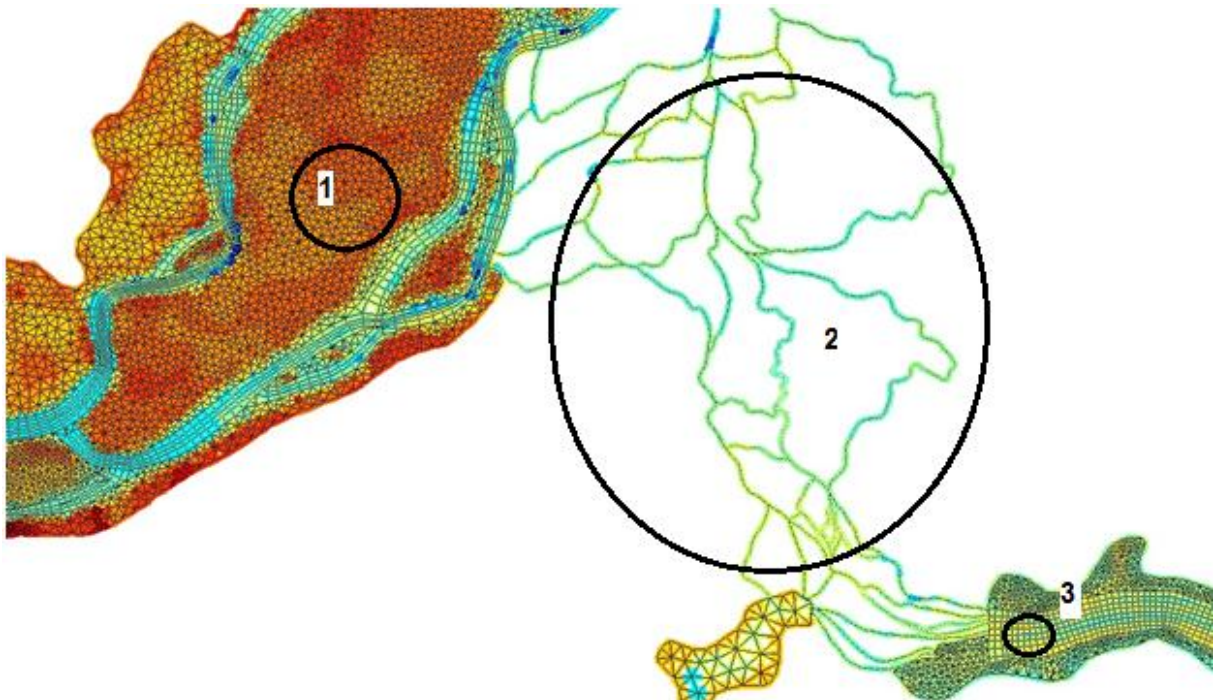


**Figure 2:** Flexible mesh grid: a combination of curvilinear mesh (3) with triangles (1), 1D channel (2) networks, etc.

The domain encompasses: the main rivers and channels of Amazon Estuary (Amazon River, Tapajós River, Xingu River, Tocantins River, Guajará Bay, Marajó Bay, Breves Strait and Pará River) and; floodplain area (Figure 3). The domain covers approximately 700 km along the coast line and 145 km offshore. It reaches 716 km upstream through the Amazon River and 430 km through Pará River/Tocantins River.

Curvilinear meshes combined with triangles and 1D channel networks were used during the mesh definition (Figure 3). The curvilinear meshes were applied to the main rivers (Amazon River, Tapajós River, Xingu River and Tocantins Rivers) and continental shelf. Triangular cells were applied to floodplain and to link curvilinear meshes with different number and size of cells. 1D channel networks were defined for small channels of Breves Strait which have width smaller than 5 km.
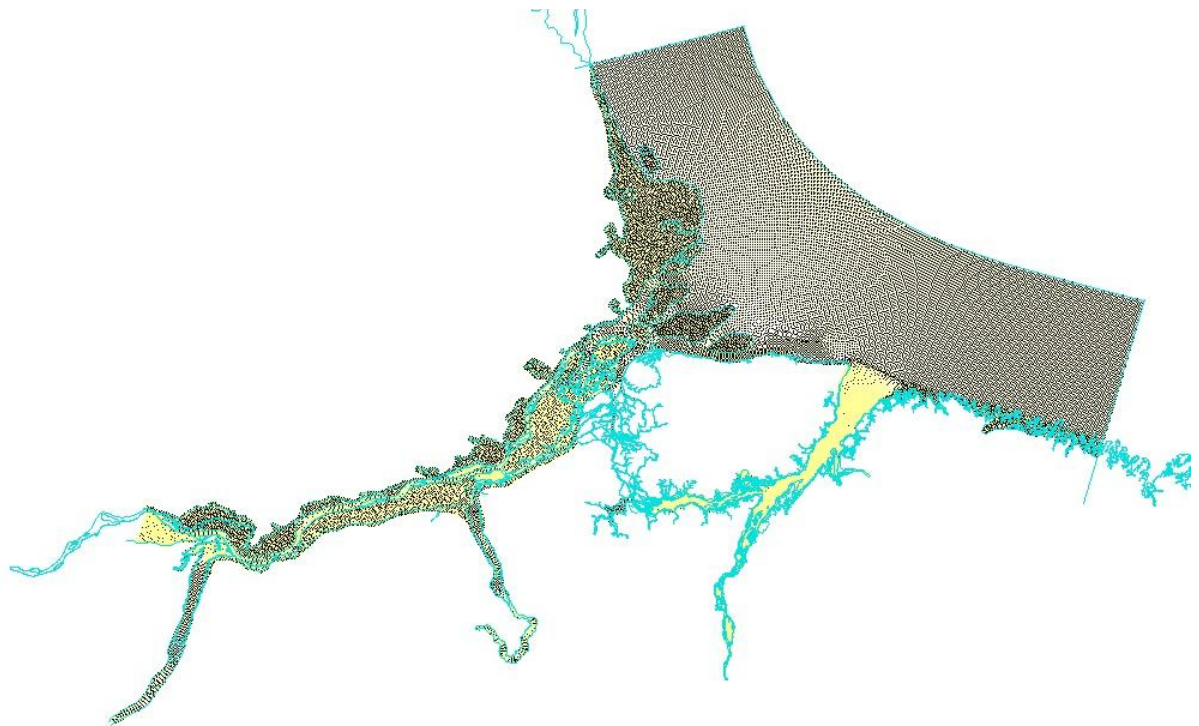


**Figure 3:** Domain and flexible mesh defined grid.

The orthogonalization parameter regarding to mesh smoothness and orthogonally presented values smaller than 0.06. The orthogonalization parameter should have the smallest value that is possible (>0) and can tolerate values up to 0.1. These orthogonality values were quite easy to find since the use of a flexible mesh.
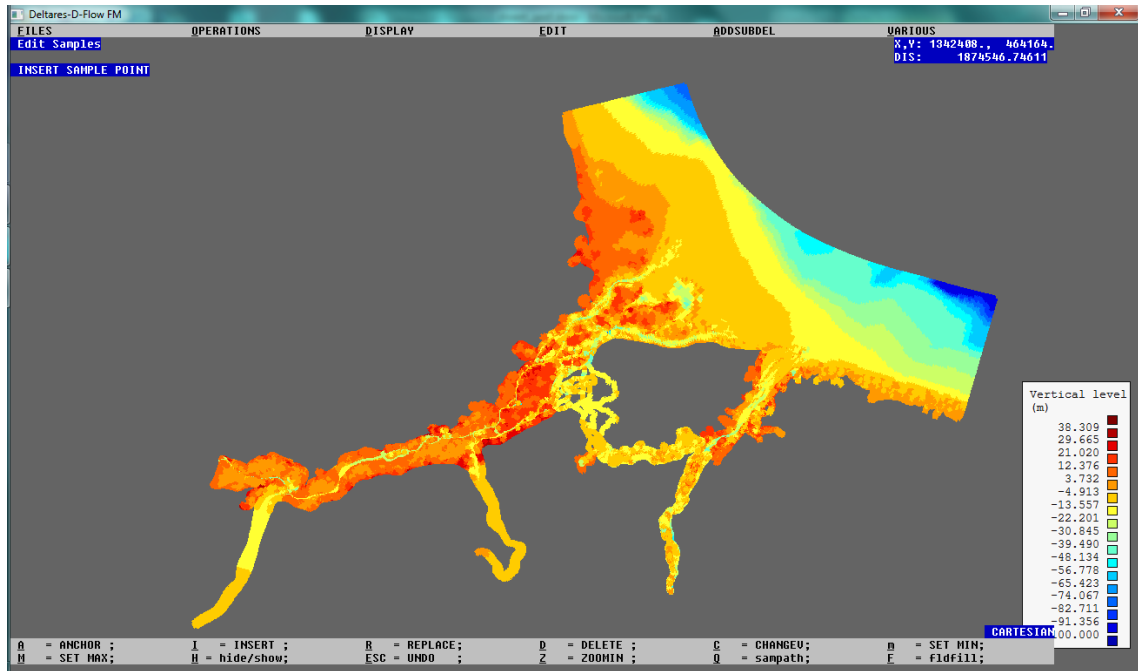
**2.2.2. Bathymetry**

The bathymetry interpolation was based on different data sets (Figure 4): charts from Brazilian Department of Hydrography and Navigation (DHN) and; bathymetry from Delft Dashboard (a MatLab-based user interface that was developed by Deltares). This second was used in order to fill missing values that are not found in nautical charts (mainly in floodplain areas).
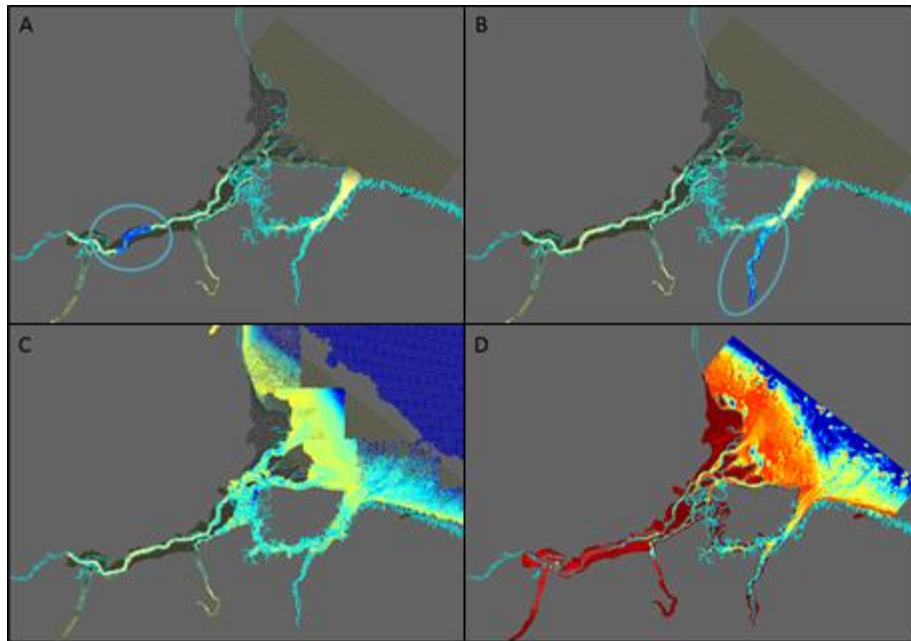


**Figure 4:** Data set that was used to bathymetry interpolation: (A) bathymetry to Amazon upstream from nautical charts from DHN website; (B) bathymetry to Tocantins River upstream from nautical charts; (C) bathymetry to Amazon Estuary and Continental shelf from nautical charts from DHN website; (D) bathymetry to entire domain obtain in Delft Dashboard.

During the calibration process, some manual corrections in the bathymetry were necessary because the size of the grid cells did not allow a reliable interpolation, for instance, sample points corresponding to sandbars (or even small islands) and deep channels were placed in a same cell, consequently, after interpolation process it resulted in shallow channels or channels abruptly blocked which generated wrong output values for water level and discharge after hydrodynamic simulations. The manual corrections were made in the cells corresponding to river channels and the continental shelf, in which, a constant and smooth slope was defined (Figure 5) by using the sample values as a guideline. It avoided abrupt changes in the bathymetry and resulted in well-defined channels.

**Figure 5:** Bathymetry after manual changes.

## 2.2.3. Roughness

Roughness coefficient means the resistance to flows in a channel or a flood plain. The Manning's coefficient was used during this research. Manning's Formula is:

$$V = \left( 1.486 \times R^{\frac{2}{3}} \times Se^{\frac{1}{2}} \right) / n$$

in which: V is the mean velocity of flow; n is Manning's roughness coefficient; R is the hydraulic radius and; Se is the slope of energy grade line.

The values of roughness coefficient were given to the domain based on Arcementjr & Schneider (1989) in which the Cowan (1956) procedure is cited. This procedure determines the effects of channel characteristics on the Manning's roughness coefficient (hereafter to be called n) value. The value of n can be determined by the formula:

$$n = (n_b + n_1 + n_2 + n_3 + n_4)m$$

in which: nb is a base value of n based on the surface material of the channel or flood plain; n1 is a correction factor regarding the effect of surface irregularities; n2 is a correction factor regarding the variations in the shape and size; n3 is a correction factor regarding the obstruction to the flow; n4 is a correction factor regarding the presence and density of

vegetation and; m is correction factor for meandering of the channel (not applicable to floodplains for which m=1).

**Table 2:** Manning's roughness coefficient defined values.

| Place | n | Brief explanation |
|---|---|---|
| Continental shelf near Amazon River mouth and Pará River Mouth | **0.015** | • **bottom composition: mud** <br> • **high suspended sediment concentration** <br> • **fluid mud** |
| Outer continental shelf | **0.022** | • **bottom composition: sand** |
| Continental shelf next to coastline (east) | **0.023** | • **bottom composition: sand** |
| Floodplain | **0.122** | • **high density of mangrove** |
| Continental shelf next to coastline (west) | **0.022** | • **bottom composition: sand** |
| Islands on Amazon River | **0.040-0.050** | • **high density of mangrove** <br> • **too high values, e.g. n=0.122, interferes in tide intrusion into the estuary.** |
| Amazon Estuary between the continental shelf and Xingu River mouth | **0.013** | • **bottom composition: mud** <br> • **high suspended sediment concentration** <br> • **fluid mud** |
| Amazon Estuary from Xingu River to Óbidos city | **0.020** | • **bottom composition: sand** |
| Tapajós River and Xingu River | **0.022** | • **bottom composition: sand** |
| Breves Streit | **0.023** | • **bottom composition: sand** <br> • **meandering degree** |
| Pará River islands | **0.030** | • **high density of mangrove** <br> • **too high values, e.g. n=0.122, interferes in tide intrusion into the estuary.** |
| Pará River | **0.017-0.020** | • **bottom composition: sand** |
| Tocantins River | **0.020-0.022** | • **bottom composition: sand** <br> • **presence of obstructions** <br> • **meandering degree** |

Base on guidelines that were given by ARCEMENTJR; SCHNEIDER (1989) the Manning's roughness coefficient definition is given (Table 2). The area regarding the continental shelf next to Amazon River mouth and Pará River mouth received a very small roughness coefficient, n=0.015, however, the smallest roughness coefficient of n=0.013 was defined to Amazon Estuary between the continental shelf and Xingu River mouth. These values were based on: the bottom is mainly composed by mud; high degree of suspended sediment; and presence of fluid mud. BEARDSLEY et al. (1995) also apply small values of roughness for these areas due to their characteristics On the other hand, the floodplain receives the biggest values of roughness, n=0.122, due to the density of mangrove in these areas. The other areas receive values around n=0.025, which varies in other to bed sediment grain size.

## 2.2.4. Discharge and sea boundaries

The rivers discharges were defined on data set that is available on National Water Agency (ANA, 2013) website. The average monthly discharge for each river was calculated by using 30 years of data (Figure 6).
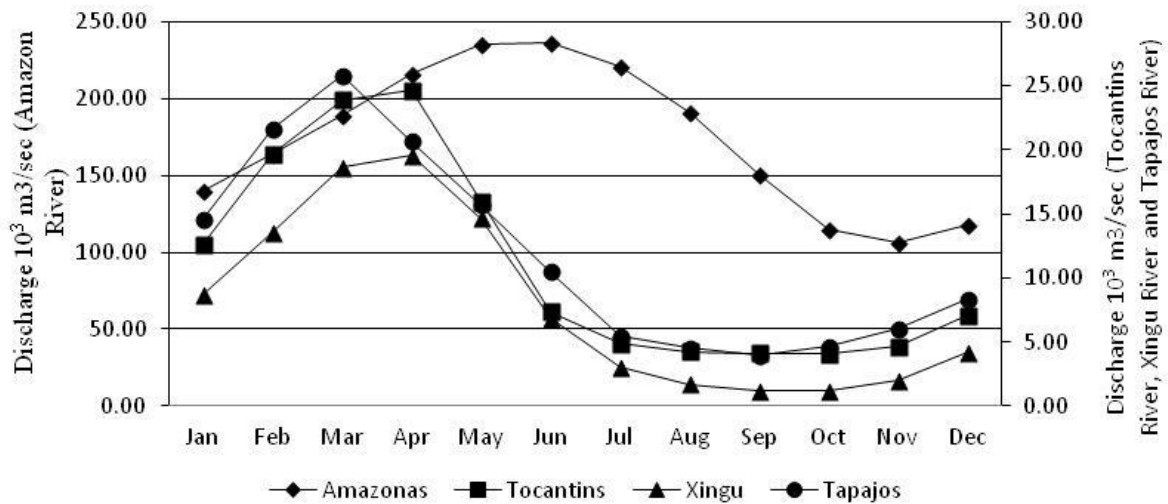


**Figure 6:** Average monthly discharge to the main river on Amazon Estuary.

The discharge data for Amazon River was taken in Óbidos city, for Tapajós River in Itaituba city, for Xingu River in Altamira city and for Tocantins River in Tucuruí city. These cities were chosen in order to avoid problems with tidal wave on upstream open boundaries since the tidal wave reaches long distances inside the river system.

The sea level boundary condition was defined based on Regional Tidal Solutions (OTIS) data for Amazon Shelf and the components used were M2, S2, N2, K1, O1 and M4. The regional inverse solution generally fit the data significantly better for complex topographic areas and in shallow water - what occurs on the continental shelf adjacent to Amazon Estuary - when it is compared with TPXO global solutions (EGBERT; EROFEEVA, 2002).

## 2.2.5. Wind

Curtin & Legeckis (1986) determines wind from the east with magnitude between 3-12 m s-1 and direction between 60-100 degrees true north based on some sampling analyses on Amazon continental shelf. The wind magnitude and direction values defined for the Amazon Estuary modelling were 12 m s-1 and 80 degrees true north. The wind was considered constant in time and space in order to make the model more controllable during the calibration process.

## 2.2.6. Time Setup

The model was set with maximum time step equal to 5 minutes and the Courant parameter used was 0.7.

The model was running into 3 different setups, each one with simulation time equal 1 month: the first to calibration, the second to simulate the dry period and the third to simulate wet period. During the calibration the considered month was July (available in situ discharge data for calibration), for dry season simulation and wet season the considered month were November and May, respectively.

## 3. Results

## 3.1. Calibration

In order to calibrate the model, 7 stations and 2 cross-sections were used (Figure 7). The stations are distributed on estuary mouth and coastline. Data for each station is available on FEMAR website. The cross-sections are located on Breves Strait and Tocantins River mouth to calibrate the flow within the estuary. For these cross-sections, data survey was made during one tidal cycle in July (wet season).



**Figure 7:** Location of stations and cross-section that was used during calibration.

Pearson's correlation coefficient and root mean square error (rmse) are the main two parameters considered during the calibration process. Tidal components analysis also was take in account during the calibration of stations and net discharge for cross-sections.

The Pearson's correlation coefficient determines linear relationship for two variables, but same correlation value can represent a set of correlations scenario, due to this the rmse were applied in order to determine the error (dimensional), thus given a better interpretation of results.

### 3.1.1. Water level calibration

The results of calibration of stations regarding water level are given on Figure 8, Figure 9, Table 3, Table 4, Table 5 and Table 6. Figure 8 shows time series plots for each station in order to compare amplitude and phase of calculated and observed signals. Figure 9 shows the signal correlation for each station. Table 3, Table 4 and Table 5 contain the amplitude of the main tidal components and Table 6 contains the statistics results.
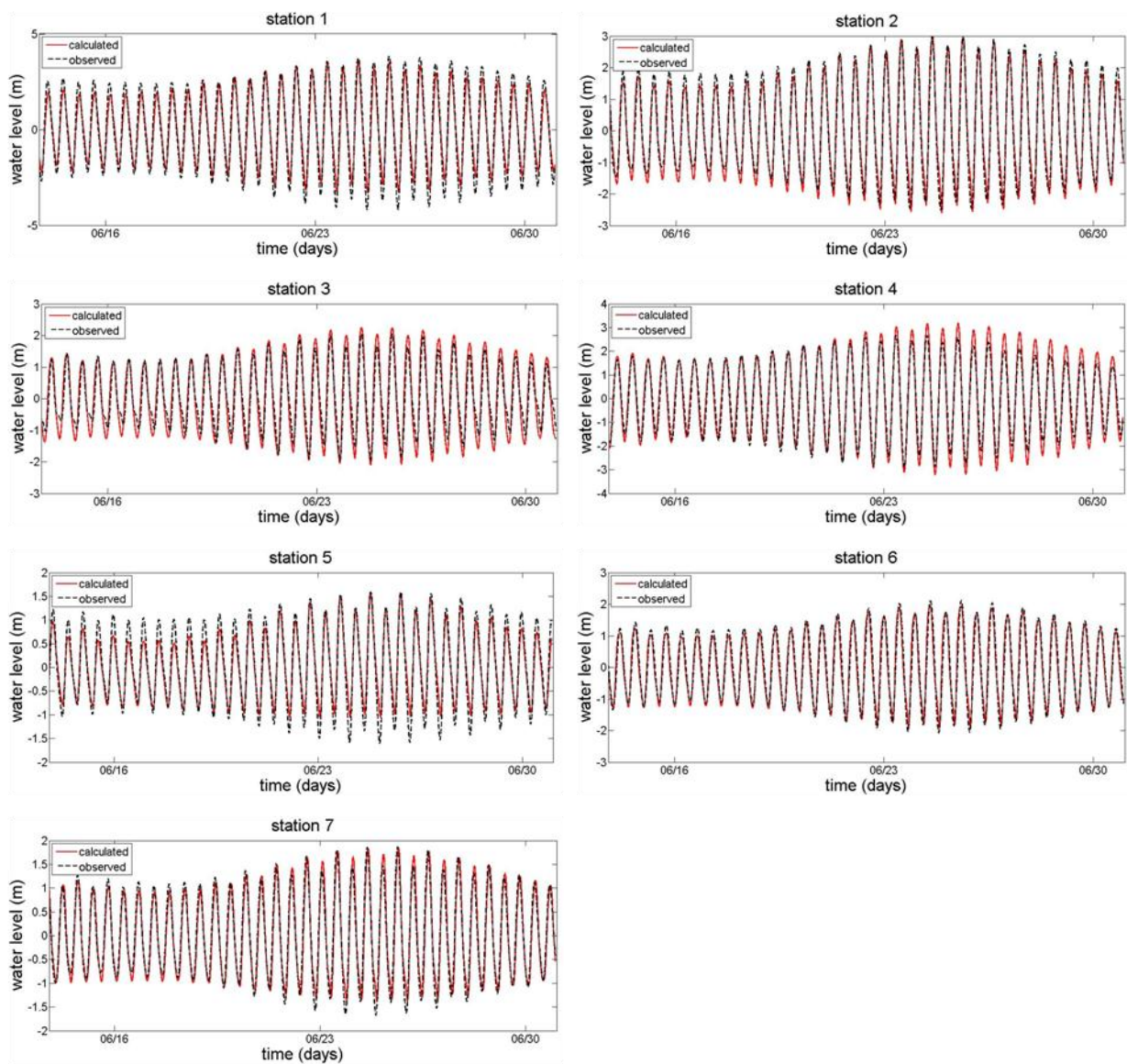


**Figure 8:** Time series comparison plot for tidal signal.

The model result was underestimated on Station 1. Around this station, the tidal range about 12 m can be reached (BEARDSLEY et al., 1995), these values were not presented by the hydrodynamic modeling. However the calculated values are in phase with calibration values. The difference of amplitude can be attributed mainly to M2 and M4.The rmse was 0.50 m that

was considered an acceptable value since the tidal range presents variation between 6 m and 9 m for the period considered.

The stations 2, 3 and 4 are located at the coastline also, but for these stations the results were overestimated, mainly during the spring tide. This variation can occur due to the difference of bathymetry and morphology between the real and simulated scenarios, since these areas present a large number of channels and small estuaries that are not present on the model. The absence of them generated an amplification of tidal range mainly during the spring tide. The difference of amplitude can be attributed mainly to MN4 and MS4 for station 2 and to M2 for stations 3 and 4. For these stations the rmse was around 0.30 m because the tidal range present values around 5m.

**Table 3:** Amplitude (amp) of tidal components O1, NO1 and K1 for calculated (cal) and observed (obs).values in meters.

|  | O1 | | NO1 | | K1 | |
| --- | --- | --- | --- | --- | --- | --- |
| **obs** | amp obs | amp cal | amp obs | amp cal | amp obs | amp cal |
| **Station 1** | 0.1368 | 0.1498 | 0.0212 | 0.0539 | 0.1612 | 0.2141 |
| **Station 2** | 0.0664 | 0.1176 | 0.0148 | 0.0351 | 0.1132 | 0.1596 |
| **Station 3** | 0.1304 | 0.0836 | 0.0146 | 0.0259 | 0.1424 | 0.1146 |
| **Station 4** | 0.1216 | 0.1074 | 0.0157 | 0.0228 | 0.1528 | 0.1474 |
| **Station 5** | 0.0589 | 0.0917 | 0.0137 | 0.0162 | 0.1308 | 0.1146 |
| **Station 6** | 0.0995 | 0.064 | 0.0129 | 0.0184 | 0.1157 | 0.084 |
| **Station 7** | 0.1083 | 0.0489 | 0.0149 | 0.0149 | 0.1253 | 0.0642 |

**Table 4**: Amplitude (amp) of tidal components N2, M2 and S2 for calculated (cal) and observed (obs) values in meters.

|  | N2 | | M2 | | S2 | |
| --- | --- | --- | --- | --- | --- | --- |
| **obs** | amp obs | amp cal | amp obs | amp cal | amp obs | amp cal |
| **Station 1** | 0.4856 | 0.3582 | 2.6899 | 2.2279 | 0.4664 | 0.3527 |
| **Station 2** | 0.3111 | 0.3081 | 1.8651 | 1.7787 | 0.3556 | 0.3415 |
| **Station 3** | 0.2255 | 0.2617 | 1.1498 | 1.4533 | 0.2819 | 0.3114 |
| **Station 4** | 0.3423 | 0.4135 | 1.8622 | 2.067 | 0.3607 | 0.5104 |
| **Station 5** | 0.1724 | 0.1338 | 1.0147 | 0.8051 | 0.1739 | 0.1419 |
| **Station 6** | 0.2259 | 0.2209 | 1.3808 | 1.3017 | 0.2881 | 0.2557 |
| **Station 7** | 0.1957 | 0.1834 | 1.1146 | 1.1017 | 0.2285 | 0.2113 |

**Table 5:** Amplitude (amp) of tidal components MN4, M4 and MS4 for calculated (cal) and observed (obs) values in meters.

| obs | MN4 | | M4 | | MS4 | |
|---|---|---|---|---|---|---|
| | amp obs | amp cal | amp obs | amp cal | amp obs | amp cal |
| **Station 1** | 0.0001 | 0.097 | 0.0416 | 0.2941 | 0.0003 | 0.1045 |
| **Station 2** | 0.0002 | 0.0874 | 0.2946 | 0.2873 | 0.0002 | 0.0901 |
| **Station 3** | 0.0004 | 0.0442 | 0.3178 | 0.1447 | 0.0003 | 0.0529 |
| **Station 4** | 0.0003 | 0.003 | 0.1075 | 0.0584 | 0.0003 | 0.0027 |
| **Station 5** | 0.0002 | 0.0504 | 0.2176 | 0.1579 | 0.0002 | 0.0507 |
| **Station 6** | 0.0003 | 0.058 | 0.0885 | 0.1648 | 0.0003 | 0.07 |
| **Station 7** | 0.0003 | 0.0485 | 0.01431 | 0.1427 | 0.0003 | 0.0535 |

The results for stations 5, located on Amazon River, present the biggest rmse in relation with the tidal range on this location (maximum of 4 m during the spring tide for the analyzed period), around 10%. This error can be attributed to the irregular bathymetry along the Amazon River that was not considered during the modelling. The tidal components M2, MN4, M4 and MS4 presented significant differences with values of 21 cm, 5 cm, 6 cm and 5 cm, respectively.

Stations 6 and 7, located on Pará River, present good calibration. These rmse get values of 20 cm what represent 5% of the local tidal range. As well as station 5, the tidal components M2, MN4, M4 and MS4 reach the biggest difference when calculated and observed values are compared. On the other hand, M4 was the main tidal component that generated the error for station 7, with a difference of 12 cm between calculated and observed values.

In general, the main differences of tidal signal are regarding the tidal components M2 as well as MN4, M4 and MS4 for that the hypothesis is the differences of bathymetry since quarter-diurnal tidal components are influenced by the interaction of the wave with the bottom (PARKER, 1991). On the other hand, the seasonality of, for instance, wind and discharge can induce variations on the tidal components response (VOINOV, 2007), considering that a constant wind in time and space, and average monthly discharges were applied during de modelling.
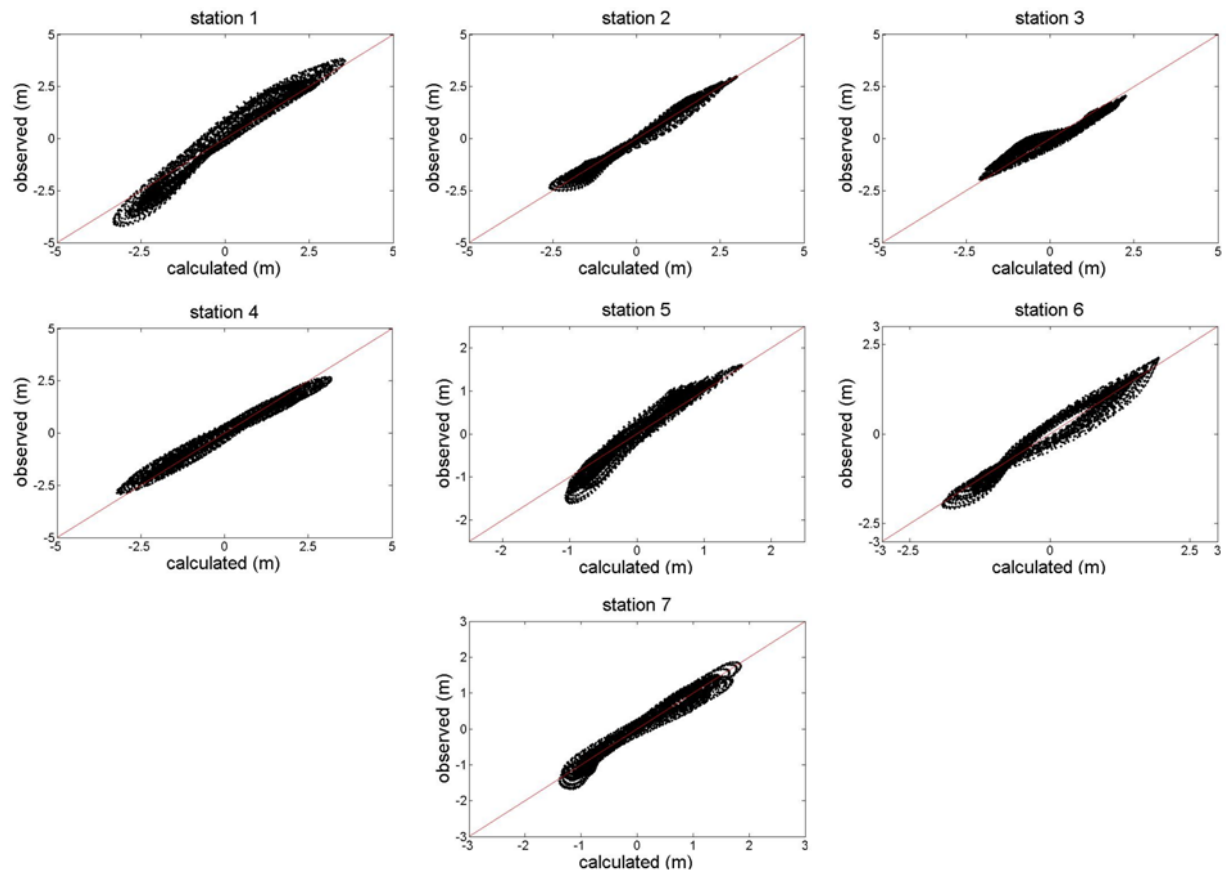
**Figure 9:** Correlation analysis for water level in which the observed and calculated values are compared.

In general, the model presents a good calibration for tidal signal since the Pearson's correlation coefficients around 0.98 were found and the rmse values are not bigger than 15% of mean local tidal range.

**Table 6:** Pearson's correlation coefficient and root mean square error for water level in which the observed and calculated values are compared.

| Station | Pearson correlation coefficient | Root mean square error (m) |
| --- | --- | --- |
| Station 1 | 0.9802 | 0.5157 |
| Station 2 | 0.9872 | 0.2283 |
| Station 3 | 0.9664 | 0.3270 |
| Station 4 | 0.9861 | 0.3061 |
| Station 5 | 0.9750 | 0.2162 |
| Station 6 | 0.9804 | 0.2072 |
| Station 7 | 0.9765 | 0.1835 |

**3.1.2. Discharge calibration**

The results of calibration of cross-sections regarding discharge are given on Figure 10, Table 7 and Table 8. Figure 8 shows time series plots for each station in order to compare amplitude and phase of calculated and observed signals. Table 7 contains the statistics results and Table 8 the net discharge for observed and calculated values during a determined period.
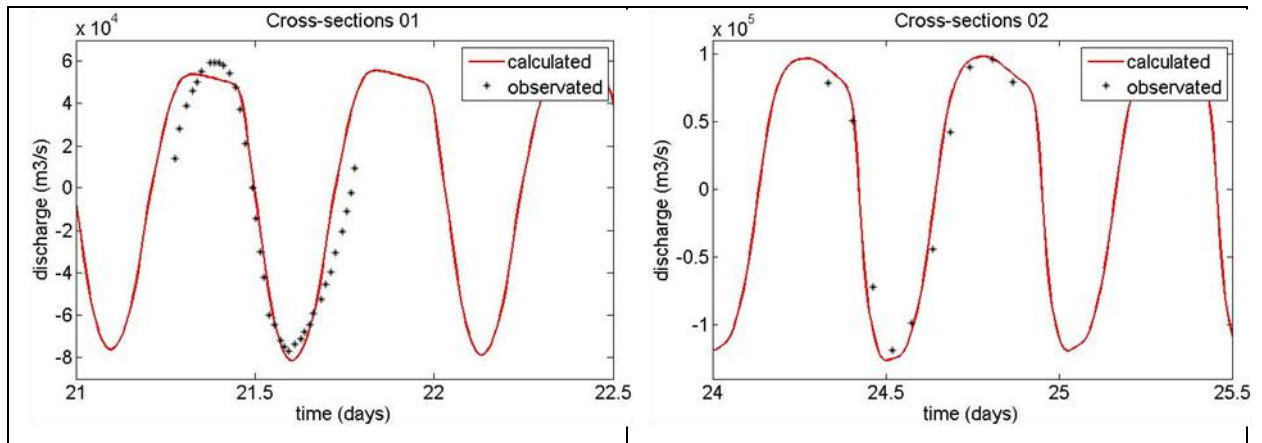


**Figure 10:** Time series comparison plot for discharge.

Analyze of cross-sections discharge shows good results of Pearson's correlation and rmse. The correlation values were bigger than 95% and the rmse smaller than 15%.In addition to this, the net discharge calculation shows that observed and calculated match in direction and magnitude.

The net discharge calculation also shows a difference in order of to 61% of the observed values for cross-section 1. This result indicates a necessity to define the mesh grid in a different way than that applied during this modelling for Breves Strait area, for instance, more detailed 1D channel, substitute the 1D channel for 2D mesh grid, or even considered the flood plain area adjacent.

On cross-section 2, in which the mesh is more detailed, the difference between calculated and observed values of net discharge was about 15% of the observed value. At this same area, the domain is represented by a mesh grid that encompasses the morphology characteristics better than that used on adjacent area of cross-section 1.

**Table 7:** Pearson's correlation coefficient and root mean square error for discharge in which the observed and calculated values are compared.

|  | **Pearson correlation coefficient** | **Root mean square error (m)** |
|---|---|---|
| **Cross-section 1** | 0.9624 | $1.5 \times 10^4$ |
| **Cross-section 2** | 0.9840 | $1.7 \times 10^4$ |

**Table 8**: Net discharge for calibration cross-sections.

|  | **observed** | **calculated** | **Period considered** |
|---|---|---|---|
| **Cross-section 1** | $-4.1334 \times 10^4$ | $-1.6453 \times 10^4$ | T1=12h |
| **Cross-section 2** | $4.7528 \times 10^5$ | $5.4078 \times 10^5$ | T2=12.96 |

In general, the model presents an acceptable calibration since the good results for Pearson's coefficient and rmse as well as the net discharge values that show same order and direction when compared with the observed. However, the analysis of time series and net discharge calculation shows that the model should be more accurate regarding morphology information about Breves Strait.

**3.2. Hydrodynamic analyses**

In order to analyze some hydrodynamic patterns of Amazon Estuary, 5 cross-sections were defined (Figure 11) within the estuary mouth to generate information about discharge in different scenarios. The scenarios are: (1) spring tide/wet season; (2) neap tide/wet season; (3) spring tide/dry season and; (4) neap tide/dry season.
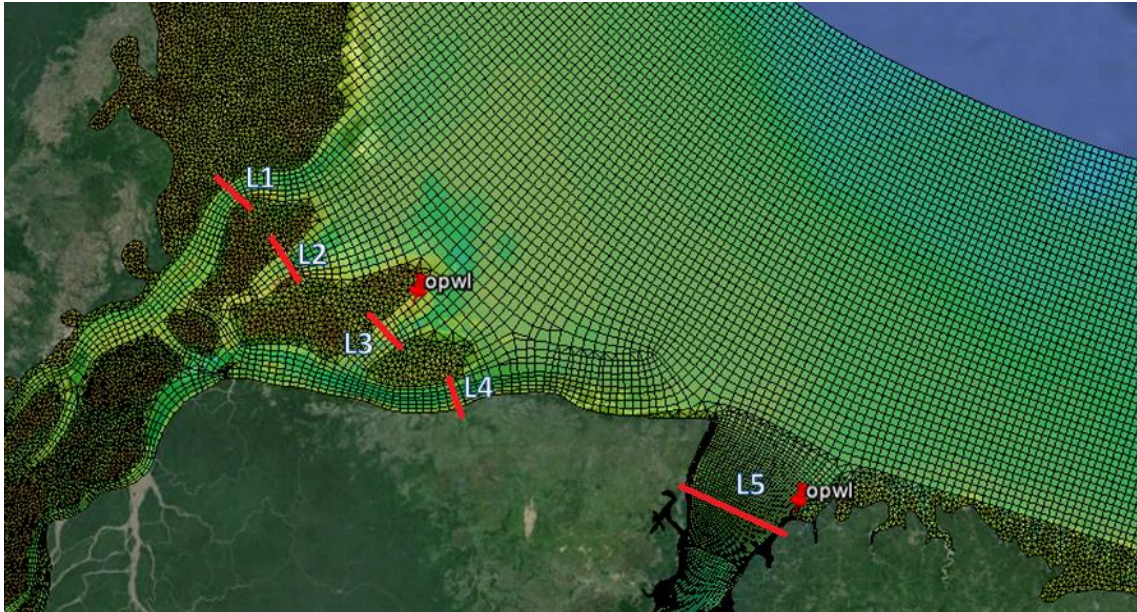
**Figure 11:** Location of the 5 cross-sections for hydrodynamic analyze and water level observation points (opwl).

The net discharge was calculated for one tidal cycle that was defined from 2 water level observed points result on estuary mouth: the first on west side of Marajó Bay and; the second on east side of Marajó Bay.
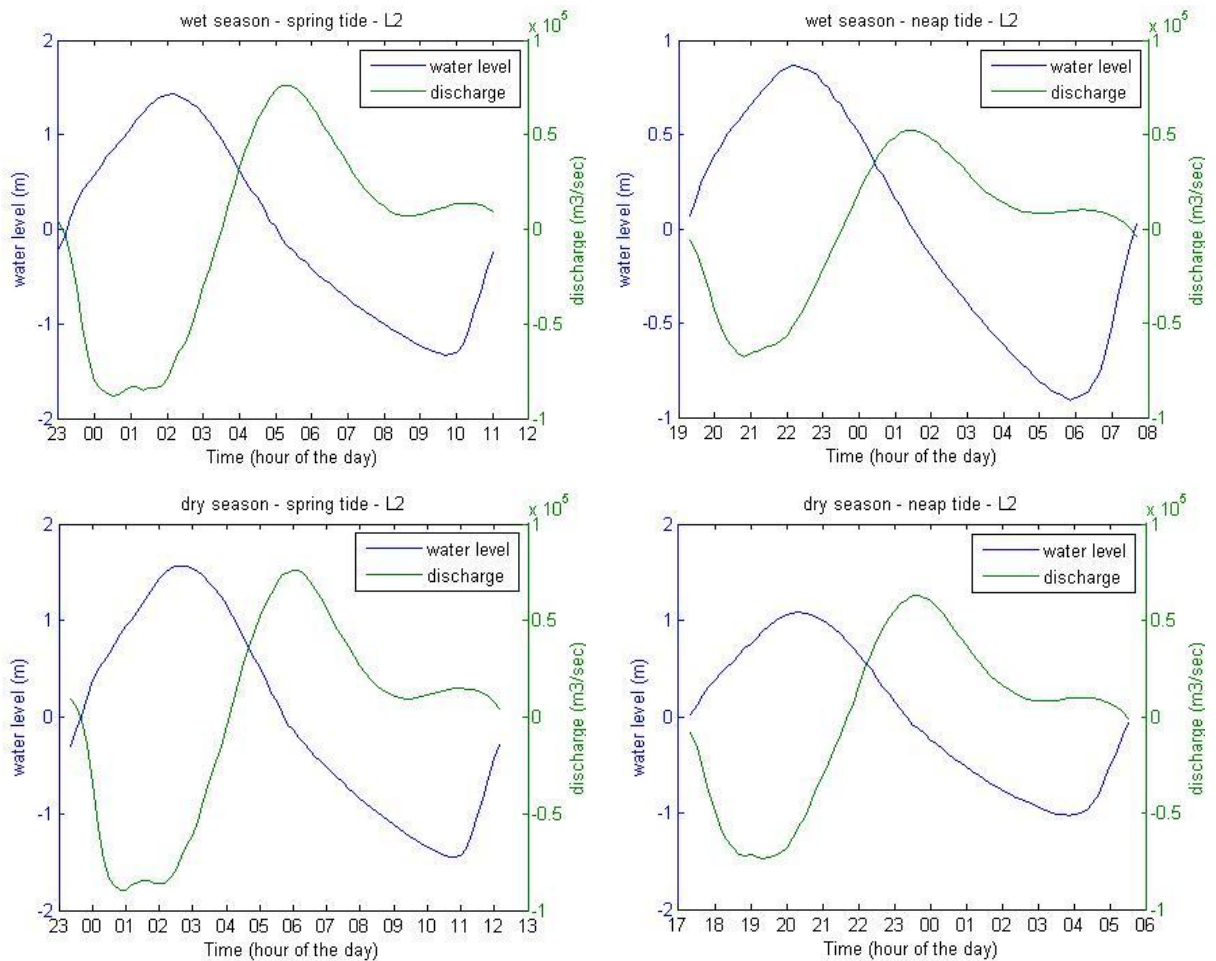
Regarding to the 4 cross-sections on the west side of Marajó Bay (Figure 12, Figure 13, Figure 14 and Figure 15), L1 and L4 presented the higher values of discharge and range than L2 and L3. They also showed small period of upstream current (negative values) for wet season what means small tidal penetration through these channels. On the other hand, L2 and L3 did not show preferential direction, but the downstream current (positive values) presents longer periods than the upstream current.
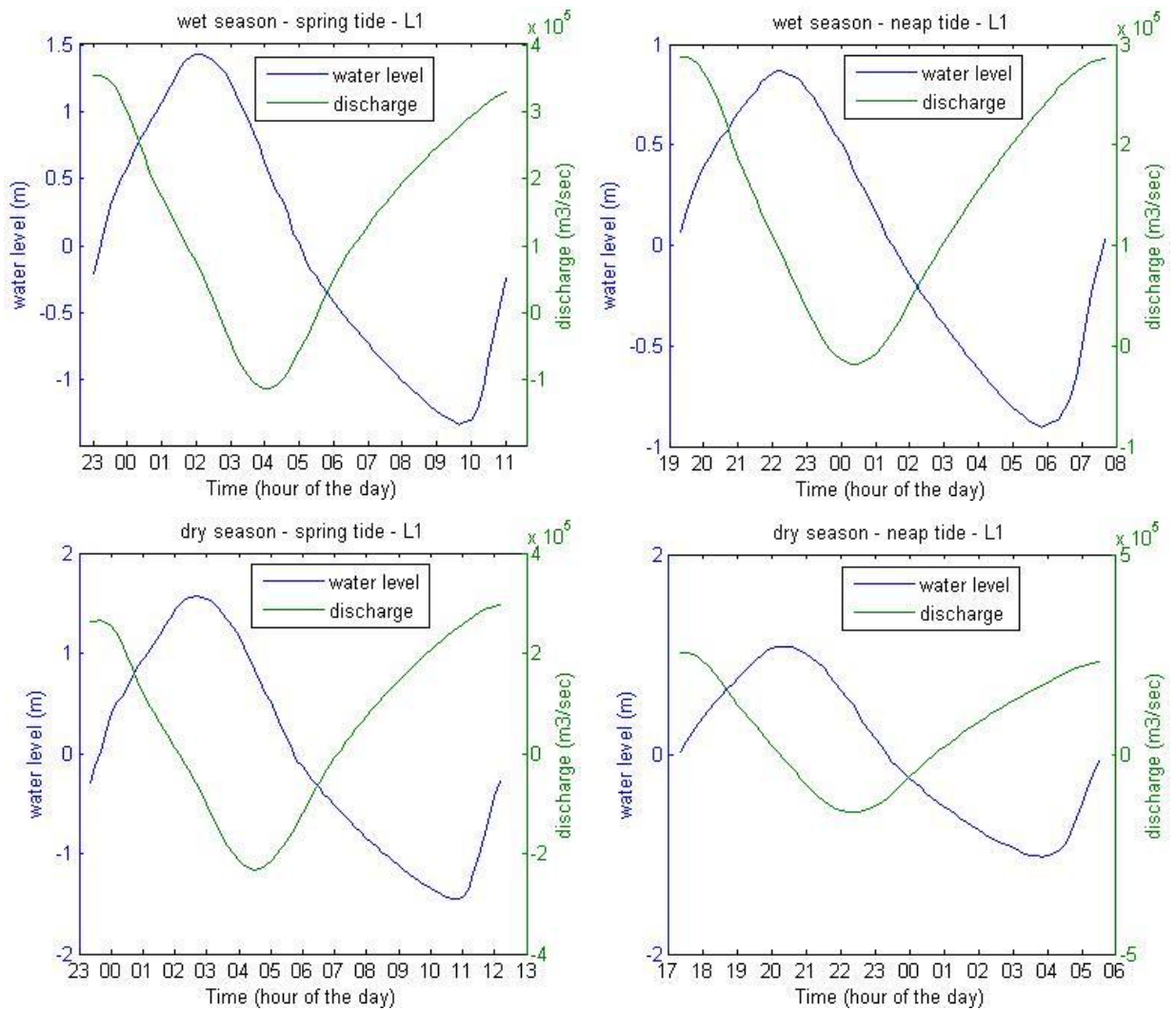
**Figure 12:** 4 scenarios of discharge for one tidal cycle for cross-section L1.

On the east side of Marajó Bay, the inversion of current direction occurs, what represents flow in upstream and downstream direction (Figure 16). The exception is at dry season for neap tide, when the discharge forces is more intense than tidal currents forces what did not allow a longer tidal penetration on this side of the estuary.
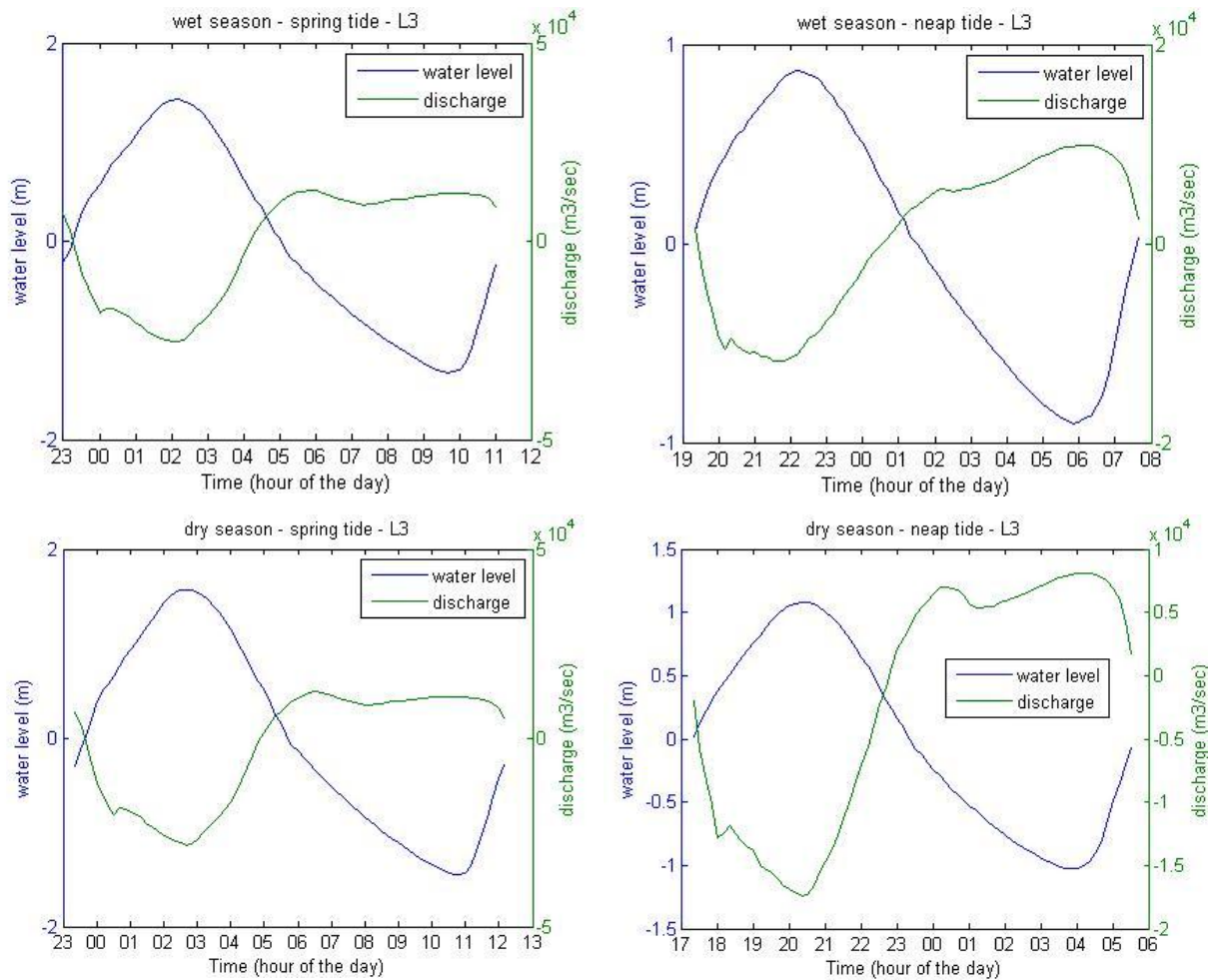
**Figure 13:** 4 scenarios of discharge for one tidal cycle for cross-section L2.

Regarding net discharge (Table 9), L1 and L4 presented positive values of net discharge, thus they are the main channels of outflow on the west side. The larger net discharge for both channels occurs during neap tide of wet season when the tidal forces is not enough to push the water inside the estuary.

L2 and L3 presented negative value of net discharge, thus they are the channels in which the tidal penetrates. The exception is in neap tide at wet season. This result can be related with grid definition, since L2 and L3 are in a shallower area and do not have well defined channels into the estuary like L1 and L4, thus the outflow flows through these latter preferably.
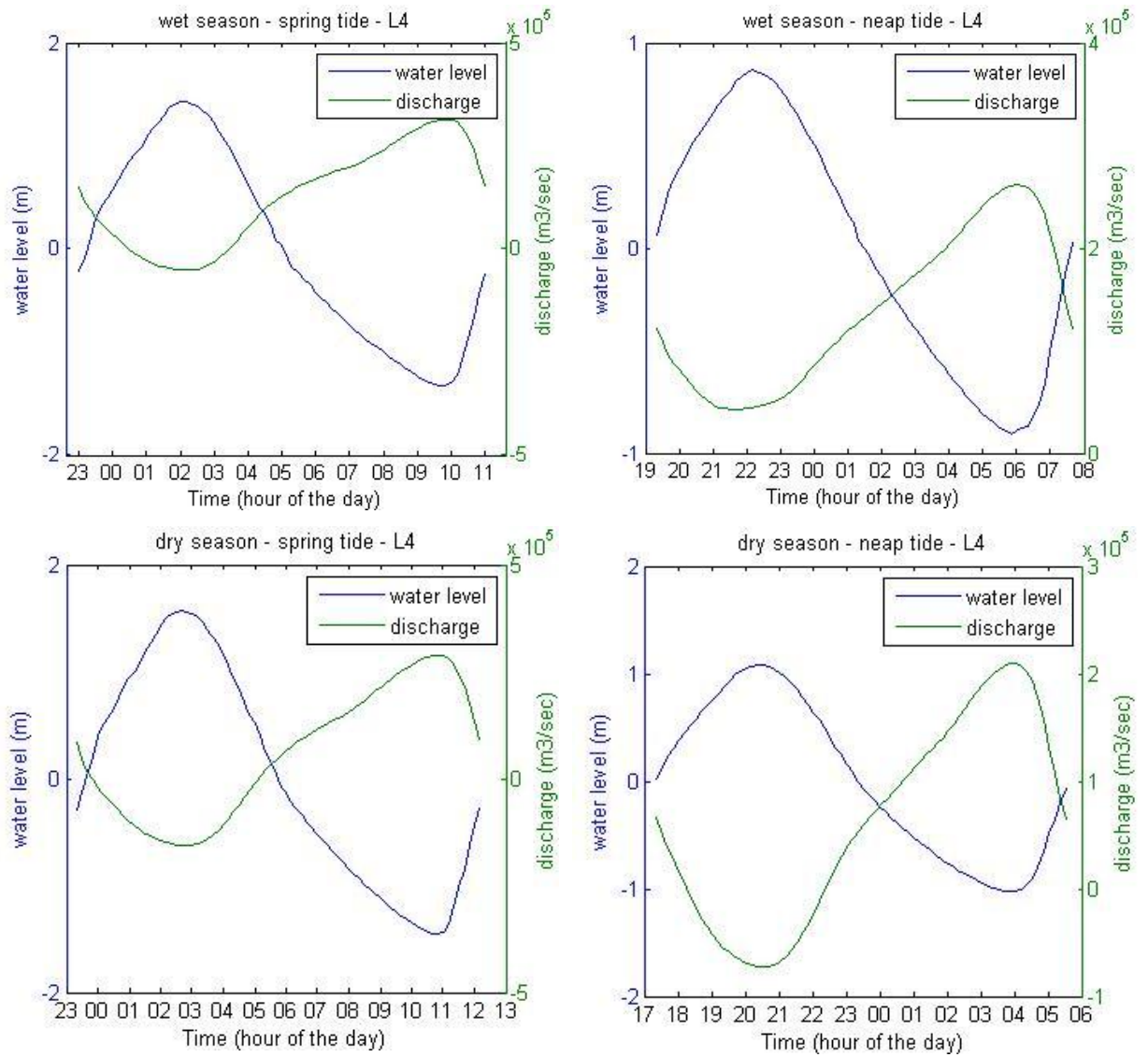
**Figure 14:** 4 scenarios of discharge for one tidal cycle for cross-section L3.

L5 presents values positives of net discharge, thus it also is an outflow channel to this estuary. Although the biggest discharge source is from Amazon river, L5 present net discharge in same order of the sum of L1, L2, L3, L4 (total net discharge on west side).

In summary, the model represented quite well the applied forces to the water into the estuary when compared with in situ observed hydrodynamic patterns. Different results due tidal variation and river discharge were possible to identify through patterns of discharge direction as well as discharge range and net discharge calculation.

**Figure 15:** 4 scenarios of discharge for one tidal cycle for cross-section L4.
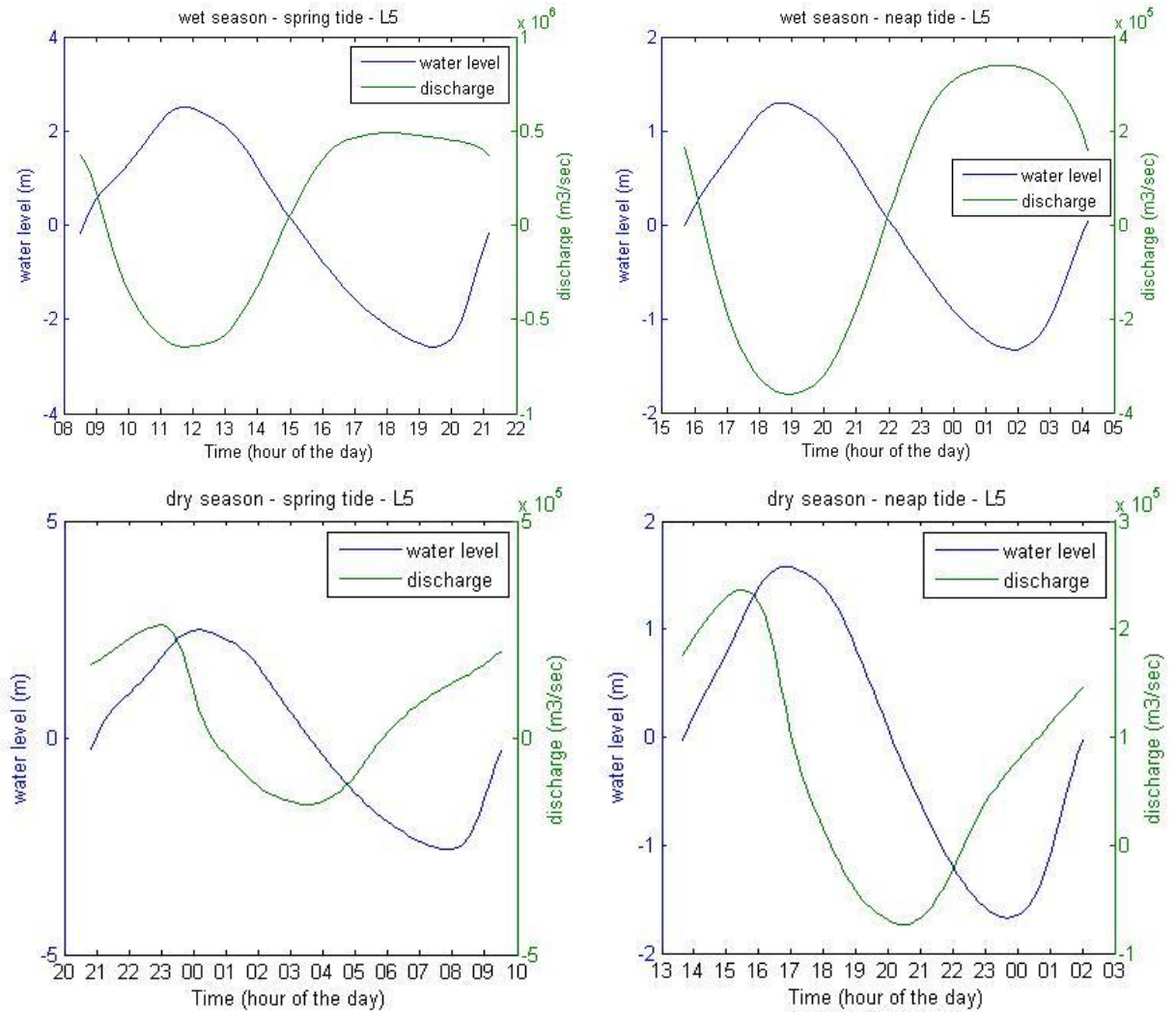
**Figure 16:** 4 scenarios of discharge for one tidal cycle for cross-section L5.

Table 9: Calculated net discharge.

| | Wet season | | Dry season | |
|---|---|---|---|---|
| **Cross-section** | Spring tide | Neap tide | Spring tide | Neap tide |
| **L1** | $9.86 \times 10^6$ | $1.05 \times 10^7$ | $4.21 \times 10^6$ | $4.13 \times 10^6$ |
| **L2** | $-1.59 \times 10^5$ | $-1.54 \times 10^4$ | $-9.94 \times 10^4$ | $-7.20 \times 10^4$ |
| **L3** | $-6.85 \times 10^4$ | $3.77 \times 10^4$ | $-1.72 \times x10^5$ | $-1.36 \times 10^5$ |
| **L4** | $9.01 \times 10^6$ | $1.03 \times 10^7$ | $4.24 \times 10^6$ | $4.43 \times 10^6$ |
| **L5** | $1.80 \times 10^6$ | $2.16 \times 10^6$ | $3.65 \times 10^6$ | $5.15 \times 10^6$ |

## 4. Summary and Conclusions

The flexible mesh model was very useful during the grid definition since it allows the representation of Amazon Estuary in a simple way, despite its complexity regarding morphology, with acceptable values of orthogonality and smoothness.

Although a coarse grid was used excluding tidal channels, channels, bars, etc., the manual changes of bathymetry helped the calibration processes, and allow the tidal signal penetration into the estuary.

The model presents a quite good calibration values for tidal signal as well as discharge since the Pearson's correlation coefficient presented values higher than 0.95 for both and rmse presented values lower than 5% for the former and 15% for the latter.

During the calibration process, the semidiurnal and quarter-diurnal components represented, significantly, the difference between observed and calculated values of water level. On the other hand, the large error of net discharge for Breves Strait shows that these channels should be better described during the grid definition.

The model also works well on representation of several scenarios that represented extreme conditions regarding tide and discharge sources of Amazon Estuary and it showed expected patterns when compared with in situ observed hydrodynamic patterns.

The model also emphasized the importance of the channel on east side of Marajó Island regarding outflow discharge to the entire system as well as the different holes of the channels on east side regarding the tidal current penetration in which the internal channels (here called L2 and L3) represented the main channels from where the coastal water flows in upstream direction due to tidal forcing.

In conclusion, the model represented quite well the Amazon Estuary even it had considered only the biggest rivers and flood plains and had ignored several smallest water bodies. The calibration results show that the model output agree with observed values in phase, magnitude and direction. In addition to this, the model also represented expected patterns.

**Acknowledgments**

**References**

Agência Nacional das Águas (ANA). 2013. HidroWeb. Disponível em: <http://hidroweb.ana.gov.br/>.

ARCEMENTJR, G. J.; SCHNEIDER, V. R. Guide for Selecting Manning's Roughness Coefficients for Natural Channels and Flood Plains. United States: 1989. v. Paper 2339

BALTAZAR, L. R. S.; MENEZES, M. O. B.; ROLLNIC, M. Contributions to the Understanding of Physical Oceanographic Processes of the Marajó Bay - PA, North Brazil. Journal of Coastal Research, n. SI 64 - Proceedings of the 11th International Coastal Symposium, p. 1443 – 1447, 2011.

BEARDSLEY, R. et al. The M2 tide on the Amazon shelf . Journal of Geophysical Research, v. 100, n. NO. C2, p. 2283–2319, 1995.

BEZERRA, M. O. et al. Physical oceanographic behavior at the Guama/Acara-Moju and the Paracauari river mouths, Amazon coast (Brazil). Journal of Coastal Research , n. SI 64 - Proceedings of the 11th International Coastal Symposium , p. 1448 – 1452, 2011.

CORRÊA, I. C. S. Aplicação do diagrama de Pejrup na interpretação da sedimentação e da dinâmica do estuário da Baía de Marajó-PA. Pesquisas em Geociências, v. 32-2, p. 109–188, 2005.

COSTA, M. H.; BOTTA, A.; CARDILLE, J. A. Effects of large-scale changes in land cover on the discharge of the Tocantins River, Southeastern Amazonia. Journal of Hydrology, v. 283, n. 1–4, p. 206–217, 2003.

COSTA, M. S. et al. Morphological and sedimentological processes of an Amazon Estuary, Maguari River (Pará - Northern Brazil). Journal of Coastal Research, n. SI 65 - Proceedings of the 12th International Coastal Symposium, p. 1110–1115, 2013.

COWAN, W. L. Estimating hydraulic roughness coefficients. Agricultural Engineering, v. 37, n. 7, p. 473–475, 1956.

CURTIN, T. B.; LEGECKIS, R. V. Physical observations in the plume region of the Amazon River during peak discharge—I. Surface variability. Continental Shelf Research, v. 6, n. 1, p. 31–51, 1986.

DAI, A.; TRENBERTH, K. E. Estimates of Freshwater Discharge from Continents: Latitudinal and Seasonal Variations. Journal of Hydrometeorology, v. 3, n. 6, p. 660–687, 2002.

EGBERT, G. D.; EROFEEVA, S. Y. Efficient inverse modeling of barotropic ocean tides. Journal of Atmospheric and Oceanic Technology, v. 19, n. 2, p. 183–204, 2002.

Fundação de Estudos do Mar (FEMAR). 2013. Catálogo de Estações Maregráficas. Disponível em: <http://www.fundacaofemar.org.br/>.

GABIOUX, M.; VINZON, S. B.; PAIVA, A. M. Tidal propagation over fluid mud layers on the Amazon shelf. Continental Shelf Research, v. 25, n. 1, p. 113–125, 2005.

GEYER, W. R. et al. Physical oceanography of the Amazon shelf. Continental Shelf Research, v. 16, n. 5–6, p. 575–616, 1996.

GREGÓRIO, A. M. DA S.; MENDES, A. C. Characterization of sedimentary deposits at the confluence of two tributaries of the Pará River estuary (Guajará Bay, Amazon). Continental Shelf Research, v. 29, n. 3, p. 609–618, 2009.

KERNKAMP, H. W. J. et al. Efficient scheme for the shallow water equations on unstructured grids with application to the Continental Shelf. Ocean Dynamics, v. 61, n. 8, p. 1175–1188, 2011.

MERTES, L. A. K.; DUNNE, T.; MARTINELLI, L. A. Channel-floodplain geomorphology along the Solimões-Amazon River, Brazil. Geological Society of America Bulletin, v. 108, n. 9, p. 1089–1107, 1996.

MIKHAILOV, V. N. Water and sediment runoff at the Amazon River mouth. Water Resources, v. 37, n. 2, p. 145–159, 2010.

MIRANDA, L. B.; CASTRO, B. M.; KJERFVE, B. Princípios de oceanografia física de estuários. São Paulo: Editora da Universidade de São Paulo, 2002.

NIKIEMA, O.; DEVENON, J.-L.; BAKLOUTI, M. Numerical modeling of the Amazon River plume. Continental Shelf Research, v. 27, n. 7, p. 873–899, 2007.

PARKER, B. B. (1991). *Tidal hydrodynamics*: John Wiley & Sons.

SIOLI, H. The Amazon and its main affluents: hydrography, morphology of the river courses, and river types. In: The Amazon. [s.l.] Springer, 1984. p. 127–165.

VINZON, S. B.; PAIVA, A. M. Modeling the sediment concentration profiles at the Amazon Shelf. In: JOHAN, C. W.; CEES, K. (Eds.). Proceedings in Marine Science. [s.l.] Elsevier, 2002. v. Volume 5p. 687–702.

VOINOV, G. (2007). Seasonal variability of the harmonic constants of the quarter-diurnal and sixth-diurnal constituents in the Barents Sea and White Sea. *Russian Meteorology and Hydrology, 32*(4), 252-261.